

**NUMERICAL ANALYSIS ON STATIC LOAD CAPACITY
OF PRESTRESSED CONCRETE SLEEPERS
UNDER HYPOTHETICAL BEARING PRESSURE DISTRIBUTION**

WAN AZLAN BIN WAN ABDUL RASHID

A project report submitted in partial fulfillment of the
requirement for the award of the degree of
Master of Engineering (Civil – Structure)

Fakulti Kejuruteraan Awam
Universiti Teknologi Malaysia

JANUARY 2012

To my beloved mother and family

ACKNOWLEDGEMENT

Countless appreciation to my mother and family who had supporting me throughout my life.

I must thank my thesis supervisor, Dr. Izni Syahrizal Ibrahim who had given me the chance to pursue this topic for my thesis. His constant support, motivation and valuable guidance were very important and I must thank him for all his time on supervising my thesis.

My special thanks to every staff and students at the Faculty of Civil Engineering at Universiti Teknologi Malaysia for all the valuable experiences and knowledge I had obtained during my study for the Masters programme at the university.

A special acknowledgement to my office mates for being very supportive and understanding during my study.

Thank you to all my friends for their joy and laughter and not to forget to anyone who had been involved directly and indirectly in developing this thesis.

This thesis is a dedication to my beloved mother and family.

ABSTRACT

Prestressed concrete sleepers are currently designed based on permissible stresses concepts resulting from quasi-static wheel loads. It was designed to exceed the mean working load to avoid loss of bond in the prestressing due to cracking of the concrete sleepers. These loads allow for static response of the sleeper due to the mechanism of vertical load transfer between the rail and sleeper as well as the sleeper and ballast interaction. In practice, the designer apply uniform pressure distribution beneath each rail seat which is dependent on the track gauge and sleeper length as stipulated in many design standards. Applying uniform pressure distribution beneath each rail seat may not be necessarily applicable to all in-situ sleepers as the contact pressure distribution between sleepers and ballast is mainly influenced by the cumulative effect of the traffic loading at various speeds over a period of time as well as the quality of ballast maintenance. A significant amount of research has been conducted by researchers worldwide over the century in postulating a set of hypothetical contact pressure distribution on the sleeper-ballast interaction. This leads to predicament as to whether the designed sleepers under the assumption of uniform contact pressure distribution had the adequate static load capacity to withstand the designed vertical loading but under different contact pressure distribution pattern. To solve this predicament, numerical analysis using commercially available finite element package, LUSAS, is carried out and comparison is made with the experimental test results in validating the finite element model. The numerical analysis will be useful in predicting the maximum vertical loading prior to the cracking of the sleeper under various hypothetical contact pressure distribution patterns. From numerical analysis, prestressed concrete sleeper that is placed on ballast has reserve strength in static load capacity with a factor between 2.2 and 2.4 of the positive rail seat test load at crack initiation.

ABSTRAK

Reka bentuk *sleeper* konkrit prategasan adalah berdasarkan kepada konsep tekanan yang dibenarkan, hasil daripada aksi beban kuasi-statik roda. Ia direka bentuk untuk melebihi purata beban kerja bagi mengelakkan kehilangan daya tarikan di dalam prategasan yang disebabkan oleh keretakan. Beban ini membenarkan respon statik oleh *sleeper* yang disebabkan oleh mekanisma perpindahan beban menegak di antara rel dan *sleeper* serta interaksi antara *sleeper* dan *ballast*. Pereka bentuk mengenakan tekanan rata yang seragam di bawah setiap kerusi rel yang bergantung kepada tolok landasan dan panjang *sleeper* seperti mana ditetapkan di dalam banyak piawaian. Menganakan tekanan yang seragam di bawah kerusi rel mungkin tidak benar untuk semua *sleeper* di landasan kerana tekanan permukaan di antara *sleeper* dan *ballast* dipengaruhi oleh kesan kumulatif daripada beban trafik pada pelbagai kelajuan pada suatu tempoh serta kualiti penyelenggaraan *ballast*. Jumlah penyelidikan yang ketara telah dilakukan oleh para penyelidik di seluruh dunia dalam menyediakan satu set hipotesis tekanan rata bagi interaksi *sleeper-ballast*. Ini membawa kepada persoalan samada reka bentuk *sleeper* dibawah andaian tekanan yang seragam mempunyai kapasiti yang mencukupi untuk menahan rekaan beban menegak tetapi di bawah pelbagai bentuk hipotesis tekanan rata. Untuk menyelesaikan persoalan ini, analisis berangka menggunakan pakej perisian komersil untuk model unsur terhingga, LUSAS, dijalankan dan perbandingan dibuat dengan keputusan daripada ujian uji kaji dalam mengesahkan penggunaan model unsur terhingga. Analisis berangka ini sangat berguna untuk meramalkan beban menegak yang maksima sebaik sebelum keretakan *sleeper* dibawah pelbagai bentuk hipotesis tekanan rata. Berdasarkan kepada keputusan analisis berangka, *sleeper* konkrit prategasan yang diletakkan di atas *ballast* mempunyai kekuatan rizab pada kapasiti beban statiknya iaitu diantara factor 2.2 dan 2.4 daripada beban ujian positif kerusi kereta api semasa keretakan mula berlaku.

TABLE OF CONTENTS

CHAPTER	TITLE	PAGE
	DEDICATION	ii
	DECLARATION	iii
	ACKNOWLEDGEMENT	iv
	ABSTRACT	v
	ABSTRAK	vi
	TABLE OF CONTENTS	vii
	LIST OF TABLES	x
	LIST OF FIGURES	xii
	LIST OF SYMBOLS	xx
	LIST OF APPENDICES	xxi
1	INTRODUCTION	1
	1.1. Modernization of the ballasted railway track network in Malaysia	1
	1.2. Functions of track components and the load path	2
	1.3. Problem statement	4
	1.4. Objectives of the study	6
	1.5. Scopes of the study	7
2	LITERATURE REVIEW	8
	2.1. Development of prestressed concrete sleepers	8
	2.2. Prestressed as the preferred concrete sleepers	9

2.3.	Load assessment on prestressed concrete sleepers	10
2.4.	Beams on elastic foundation and the ballast stiffness	13
2.5.	The centre negative moment test experiment	15
2.6.	Nonlinear finite element model of railway prestressed concrete sleeper	18
2.7.	Current practice in the theoretical analysis to design sleepers	22
3	RESEARCH METHODOLOGY	24
3.1.	Introduction	24
3.2.	Finite element model for the centre negative moment experimental setup	25
3.2.1.	Creating a new model	25
3.2.2.	Defining the geometry	26
3.2.3.	Defining the mesh – prestressing tendon	29
3.2.4.	Defining the mesh – concrete	30
3.2.5.	Defining the geometric properties	31
3.2.6.	Defining the material properties – prestressing tendon	32
3.2.7.	Defining the material properties – concrete	34
3.2.8.	Assigning attributes to the prestressing tendons	36
3.2.9.	Assigning attributes to the concrete	38
3.2.10.	Supports – Centre negative moment experimental setup	40
3.2.11.	Loading – Self weight	42
3.2.12.	Loading – Initial strain on prestressing tendons	43
3.2.13.	Loading – Vertical point load setup for the centre negative moment test	45

	3.2.14. Nonlinear control	47
	3.2.14.1. Loadcase 1	48
	3.2.14.2. Loadcase 2	50
	3.2.15. Running the analysis	52
	3.2.16. Viewing the results	53
	3.3. Finite element model with the hypothetical bearing pressure distribution patterns	58
	3.3.1. Support – Hypothetical bearing pressure distribution patterns	58
4	RESULTS, ANALYSIS AND DISCUSSIONS	62
	4.1. Validation of LUSAS' nonlinear finite element model	62
	4.2. Numerical analysis on static load capacity of the prestressed concrete sleepers under hypothetical bearing pressure distribution	64
	4.2.1. Cracking load, ultimate load and crack patterns	65
	4.2.2. Load-deflection response at first crack section	67
	4.2.3. Vertical deflection along the sleeper's length	68
	4.2.4. Principal stress distribution in x- direction on first crack section	70
	4.3. Summary of static load capacity of the prestressed concrete sleepers under hypothetical bearing pressure distribution	72
5	CONCLUSIONS AND RECOMMENDATIONS	75
	5.1. Conclusions	75
	5.2. Recommendations	76
	REFERENCES	77
	APPENDICES	80

LIST OF TABLES

TABLE NO.	TITLE	PAGE
2.1	Hypothetical bearing pressure distribution of sleeper (Sadeghi, 2005)	12
2.2	Material models used by Kaewunruen and Remennikov (2006b) in ANSYS	20
4.1	Numerical analysis results of LUSAS' nonlinear finite element model on the cracking load, ultimate load and crack patterns of the prestressed concrete sleeper under hypothetical bearing pressure distributions	66
4.2	Maximum vertical deflections and comparison with previous work by Sadeghi (2005)	69
4.3	Maximum principal stress in x-direction and comparison with previous work by Sadeghi (2005)	71
4.4	Static load capacity between test and numerical analysis	74
A.1	Input for the line geometry in LUSAS	80
A.2.1.1.	Laboratory test (Sadeghi, 2005)	83
A.2.1.2.	Input for spring support stiffness distribution in LUSAS	83
A.2.1.3.	Summary of results at first crack point	84
A.2.2.1.	Tamped either side of rail (Sadeghi, 2005)	86
A.2.2.2.	Input for spring support stiffness distribution in LUSAS	86
A.2.2.3.	Summary of results at first crack point	87
A.2.3.1.	Principal bearing on rails (Sadeghi, 2005)	89
A.2.3.2.	Input for spring support stiffness distribution in LUSAS	89
A.2.3.3.	Summary of results at first crack point	90

A.2.4.1.	Maximum intensity at the ends (Sadeghi, 2005)	92
A.2.4.2.	Input for spring support stiffness distribution in LUSAS	92
A.2.4.3.	Summary of results at first crack point	93
A.2.5.1.	Maximum intensity in the middle (Sadeghi, 2005)	95
A.2.5.2.	Input for spring support stiffness distribution in LUSAS	95
A.2.5.3.	Summary of results at first crack point	96
A.2.6.1.	Center bound (Sadeghi, 2005)	98
A.2.6.2.	Input for spring support stiffness distribution in LUSAS	98
A.2.6.3.	Summary of results at first crack point	99
A.2.7.1.	Flexure of sleeper produces variations form (Sadeghi, 2005)	101
A.2.7.2.	Input for spring support stiffness distribution in LUSAS	101
A.2.7.3.	Summary of results at first crack point	102
A.2.8.1.	Well tamped sides (Sadeghi, 2005)	104
A.2.8.2.	Input for spring support stiffness distribution in LUSAS	104
A.2.8.3.	Summary of results at first crack point	105
A.2.9.1.	Stabilized rail seat and sides (Sadeghi, 2005)	107
A.2.9.2.	Input for spring support stiffness distribution in LUSAS	107
A.2.9.3.	Summary of results at first crack point	108
A.2.10.1.	Uniform pressure (Sadeghi, 2005)	110
A.2.10.2.	Input for spring support stiffness distribution in LUSAS	110
A.2.10.3.	Summary of results at first crack point	111

LIST OF FIGURES

FIGURE NO.	TITLE	PAGE
1.1	Cross sectional layout of a typical ballasted track (Selig & Waters, 1994)	2
2.1	Deflections of elastic foundations under uniform pressure: a- Winkler foundation; b- practical soil foundation (Teodoru, 2009)	13
2.2	Load distribution region in continuous granular ballast (Zhai et al., 2004)	14
2.3	Model of ballast under one rail support point (Zhai et al., 2004)	14
2.4	The modified model of the ballast (Zhai et al., 2004)	14
2.5	Schematic diagram of centre negative moment test experiment (AS 1085.14-2003)	15
2.6	Load-deflection results by Kaewunruen and Remennikov (2006a)	16
2.7	Multi-linear stress-strain curve of concrete by Kaewunruen and Remennikov (2006a)	17
2.8	Multi-linear stress-strain curve of prestressing tendon by Kaewunruen and Remennikov (2006a)	18
2.9	Finite element model of prestressed concrete sleeper by Kaewunruen and Remennikov (2006b)	19
2.10	Model for reinforcement in finite element model (Tavarez, 2001): a) discrete; and b) smeared	20

2.11	Load-deflection response of experimental and model of the prestressed concrete sleeper by Kaewunruen and Remennikov (2006b)	21
3.1	Inputs for <i>File details</i> and <i>Model details</i> in <i>New Model</i> window	26
3.2	Selected segments of Line geometry	26
3.3	Surface geometry creation by line sweeping	27
3.4	Surface geometry of concrete excluding the increased section at the rail seat	27
3.5	Increased section at the rail seat	28
3.6	Surface geometry for the chamfer at rail seat	28
3.7	Structural bar element definition for the line mesh to model the prestressing tendons	29
3.8	Structural plane stress element definition for the surface mesh to model the concrete	30
3.9	The cross sectional area to model the geometric line for <i>4 nos. prestressing tendons</i>	31
3.10	The concrete thickness to model the Geometric Surface for the concrete	32
3.11	The isotropic material properties of the prestressing tendon in elastic region	33
3.12	The isotropic material properties of the prestressing tendon in plastic region using <i>von Mises Stress Potential model</i>	34
3.13	The isotropic material properties of the concrete in elastic region	35
3.14	The isotropic material properties of the concrete in plastic region using <i>Concrete model (Model 94)</i>	36
3.15	Selection of lines geometry that represents the prestressing tendons	37
3.16	The assigned properties on the selected line elements	37
3.17	Selection of surface geometry that represents the concrete	38

3.18	The meshed surface's plane stress elements	38
3.19	Selection of line geometry for non-structural line element (<i>None 40 mm</i>) assignment	39
3.20	Selection of line geometry for non-structural line element (<i>None 1 spacing</i>) assignment	39
3.21	Surface's plane stress elements with low aspect ratio and 90 degrees quadrilateral shape and the model dimensions in LUSAS	39
3.22	Rotate attributes in <i>Move</i> window	40
3.23	Structural support definition	41
3.24	The assigned structural support on the model	41
3.25	<i>Body Force</i> for the <i>Self Weight</i>	42
3.26	<i>Loading Assignment</i> for the <i>Self Weight</i>	43
3.27	The assigned <i>Self Weight</i> loading on the model	43
3.28	The <i>Initial Strain</i> loading on the prestressing tendons	44
3.29	<i>Loading Assignment</i> for the <i>Initial Strain</i>	44
3.30	The assigned <i>Initial Strain</i> loading on the model	45
3.31	The <i>Vertical Point Load</i> attributes	46
3.32	<i>Loading Assignment</i> for the <i>Vertical Point Load</i>	46
3.33	The assigned <i>Vertical Point Load</i> on the model	47
3.34	The incremental-iterative method for nonlinear solution	47
3.35	The nonlinear control of loadcase selection	48
3.36	The nonlinear control for <i>Loadcase 1</i>	49
3.37	The <i>Advanced</i> nonlinear control for <i>Loadcase 1</i>	50
3.38	The nonlinear control for <i>Loadcase 2</i>	51
3.39	The selected point at midspan to be set with <i>Termination criteria</i>	51
3.40	The <i>Advanced</i> nonlinear control for <i>Loadcase 2</i>	52
3.41	Setting the <i>Increment Load Factor</i> to active	53
3.42	The deformed mesh	54
3.43	The nodal number	54

3.44	Load-deflection response form the <i>Graph Wizard</i>	55
3.45	Principal stress distribution in global x-direction (SX)	56
3.46	Crack pattern on the model	56
3.47	<i>Animation Wizard</i> to display animated results of all loadcase	57
3.48	Compressing the animation using <i>Microsoft Video 1</i> compressor	57
3.49	Identification of line segments	58
3.50	Spring support stiffness' <i>Line Variation</i> inputs for <i>Segments 3</i>	59
3.51	Selecting <i>Segment 3</i> as the <i>Variation Attribute</i> for the spring support stiffness	60
3.52	Structural supports to represent the ballast stiffness at <i>Segment 3</i>	60
3.53	Spring support that represents the ballast stiffness for <i>Principal bearing on rails</i> scenario	61
4.1	Comparisons of load-deflection response between experimental results and LUSAS model	63
4.2	Load-deflection response at first crack point	67
4.3	Vertical deflection along the sleeper's length	68
4.4	Principal stress in x-direction on the first crack section	70
A.1.	Model dimensions in LUSAS	80
A.2.1.1.	Hypothetical bearing pressure distribution patterns (LUSAS model)	83
A.2.1.2.	Unloaded with external load	84
A.2.1.3.	At initiation of crack (external load = 485 kN)	84
A.2.1.4.	At ultimate state (external load = 649 kN)	84
A.2.1.5.	Load-deflection relation for first crack point (Node no.54 at bottom of railseat)	84
A.2.1.6.	Vertical deflection along the sleeper length at different load stage	85
A.2.1.7.	Principal stress in x-direction at first crack section (Node no.54 at bottom of railseat)	85

A.2.2.1.	Hypothetical bearing pressure distribution patterns (LUSAS model)	86
A.2.2.2.	Unloaded with external load	87
A.2.2.3.	At initiation of crack (external load = 435 kN)	87
A.2.2.4.	At ultimate state (external load = 658 kN)	87
A.2.2.5.	Load-deflection relation for first crack point (Node no.54 at bottom of railseat)	87
A.2.2.6.	Vertical deflection along the sleeper length at different load stage	88
A.2.2.7.	Principal stress in x-direction at first crack section (Node no.54 at bottom of railseat)	88
A.2.3.1.	Hypothetical bearing pressure distribution patterns (LUSAS model)	89
A.2.3.2.	Unloaded with external load	90
A.2.3.3.	At initiation of crack (external load = 485 kN)	90
A.2.3.4.	At ultimate state (external load = 645 kN)	90
A.2.3.5.	Load-deflection relation for first crack point (Node no.54 at bottom of railseat)	90
A.2.3.6.	Vertical deflection along the sleeper length at different load stage	91
A.2.3.7.	Principal stress in x-direction at first crack section (Node no.54 at bottom of railseat)	91
A.2.4.1.	Hypothetical bearing pressure distribution patterns (LUSAS model)	92
A.2.4.2.	Unloaded with external load	93
A.2.4.3.	At initiation of crack (external load = 455 kN)	93
A.2.4.4.	At ultimate state (external load = 652 kN)	93
A.2.4.5.	Load-deflection relation for first crack point (Node no.54 at bottom of railseat)	93
A.2.4.6.	Vertical deflection along the sleeper length at different load stage	94
A.2.4.7.	Principal stress in x-direction at first crack section (Node no.54 at bottom of railseat)	94

A.2.5.1.	Hypothetical bearing pressure distribution patterns (LUSAS model)	95
A.2.5.2.	Unloaded with external load	96
A.2.5.3.	At initiation of crack (external load = 460 kN)	96
A.2.5.4.	At ultimate state (external load = 653 kN)	96
A.2.5.5.	Load-deflection relation for first crack point (Node no.54 at bottom of railseat)	96
A.2.5.6.	Vertical deflection along the sleeper length at different load stage	97
A.2.5.7.	Principal stress in x-direction at first crack section (Node no.54 at bottom of railseat)	97
A.2.6.1.	Hypothetical bearing pressure distribution patterns (LUSAS model)	98
A.2.6.2.	Unloaded with external load	99
A.2.6.3.	At initiation of crack (external load = 485 kN)	99
A.2.6.4.	At ultimate state (external load = 648 kN)	99
A.2.6.5.	Load-deflection relation for first crack point (Node no.54 at bottom of railseat)	99
A.2.6.6.	Vertical deflection along the sleeper length at different load stage	100
A.2.6.7.	Principal stress in x-direction at first crack section (Node no.54 at bottom of railseat)	100
A.2.7.1.	Hypothetical bearing pressure distribution patterns (LUSAS model)	101
A.2.7.2.	Unloaded with external load	102
A.2.7.3.	At initiation of crack (external load = 455 kN)	102
A.2.7.4.	At ultimate state (external load = 647 kN)	102
A.2.7.5.	Load-deflection relation for first crack point (Node no.54 at bottom of railseat)	102
A.2.7.6.	Vertical deflection along the sleeper length at different load stage	103

A.2.7.7.	Principal stress in x-direction at first crack section (Node no.54 at bottom of railseat)	103
A.2.8.1.	Hypothetical bearing pressure distribution patterns (LUSAS model)	104
A.2.8.2.	Unloaded with external load	105
A.2.8.3.	At initiation of crack (external load = 255 kN)	105
A.2.8.4.	At ultimate state (external load = 347 kN)	105
A.2.8.5.	Load-deflection relation for first crack point (Node no. 1168 at top chamfer)	105
A.2.8.6.	Vertical deflection along the sleeper length at different load stage	106
A.2.8.7.	Principal stress in x-direction at first crack section (Node no. 1168 at top chamfer)	106
A.2.9.1.	Hypothetical bearing pressure distribution patterns (LUSAS model)	107
A.2.9.2.	Unloaded with external load	108
A.2.9.3.	At initiation of crack (external load = 480 kN)	108
A.2.9.4.	At ultimate state (external load = 644 kN)	108
A.2.9.5.	Load-deflection relation for first crack point (Node no.54 at bottom of railseat)	108
A.2.9.6.	Vertical deflection along the sleeper length at different load stage	109
A.2.9.7.	Principal stress in x-direction at first crack section (Node no.54 at bottom of railseat)	109
A.2.10.1.	Hypothetical bearing pressure distribution patterns (LUSAS model)	110
A.2.10.2.	Unloaded with external load	111
A.2.10.3.	At initiation of crack (external load = 475 kN)	111
A.2.10.4.	At ultimate state (external load = 647 kN)	111
A.2.10.5.	Load-deflection relation for first crack point (Node no.54 at bottom of railseat)	111
A.2.10.6.	Vertical deflection along the sleeper length at different load stage	112

A.2.10.7.	Principal stress in x-direction at first crack section (Node no.54 at bottom of railseat)	112
A.3.1.	Schematic diagram of rail seat negative moment test (AS 1085.14-2003)	115
A.3.2.	Schematic diagram of rail seat positive moment test (AS 1085.14-2003)	116

LIST OF SYMBOLS

K_b	-	Ballast stiffness
h_b	-	Depth of ballast
l_e	-	Effective supporting length of half sleeper
l_b	-	Width of sleeper underside
α	-	Ballast stress distribution angle
E_b	-	Elastic modulus of the ballast
f_c'	-	Specified compressive strength of concrete
E_c	-	Elastic modulus of the concrete
f_{ct}'	-	Tensile strength of the concrete
L1	-	Unloaded with external load
L2	-	Load at initiation of crack
L3	-	Load at ultimate state
D	-	Diameter of prestressing tendon
A_s	-	Area of prestressing tendon

LIST OF APPENDICES

APPENDIX	TITLE	PAGE
1.A.	Model dimensions and input for the line geometry	80
1.B.	Cross sectional area of prestressing tendons (A_s)	81
1.C.	Modulus of elasticity of concrete (E_c)	81
1.D.	Ballast stiffness for the spring supports (k_b)	82
2.1.A.	Spring support stiffness input for <i>Laboratory test</i>	83
2.1.B.	Principal stress distribution in x-direction and crack pattern	84
2.1.C.	Load-deflection at first crack point	84
2.1.D.	Vertical deflection along the sleeper length at different load stage	85
2.1.E.	Principal stress in x-direction on the first crack section	85
2.2.A.	Spring support stiffness input for <i>Tamped either side of rail</i>	86
2.2.B.	Principal stress distribution in x-direction and crack pattern	87
2.2.C.	Load-deflection at first crack point	87
2.2.D.	Vertical deflection along the sleeper length at different load stage	88
2.2.E.	Principal stress in x-direction on the first crack section	88
2.3.A.	Spring support stiffness input for <i>Principal bearing on rails</i>	89
2.3.B.	Principal stress distribution in x-direction and crack pattern	90
2.3.C.	Load-deflection at first crack point	90

2.3.D.	Vertical deflection along the sleeper length at different load stage	91
2.3.E.	Principal stress in x-direction on the first crack section	91
2.4.A.	Spring support stiffness input for <i>Maximum intensity at the ends</i>	92
2.4.B.	Principal stress distribution in x-direction and crack pattern	93
2.4.C.	Load-deflection at first crack point	93
2.4.D.	Vertical deflection along the sleeper length at different load stage	94
2.4.E.	Principal stress in x-direction on the first crack section	94
2.5.A.	Spring support stiffness input for <i>Maximum intensity in the middle</i>	95
2.5.B.	Principal stress distribution in x-direction and crack pattern	96
2.5.C.	Load-deflection at first crack point	96
2.5.D.	Vertical deflection along the sleeper length at different load stage	97
2.5.E.	Principal stress in x-direction on the first crack section	97
2.6.A.	Spring support stiffness input for <i>Center bound</i>	98
2.6.B.	Principal stress distribution in x-direction and crack pattern	99
2.6.C.	Load-deflection at first crack point	99
2.6.D.	Vertical deflection along the sleeper length at different load stage	100
2.6.E.	Principal stress in x-direction on the first crack section	100
2.7.A.	Spring support stiffness input for <i>Flexure of sleeper produces variations form</i>	101
2.7.B.	Principal stress distribution in x-direction and crack pattern	102
2.7.C.	Load-deflection at first crack point	102
2.7.D.	Vertical deflection along the sleeper length at different load stage	103

2.7.E.	Principal stress in x-direction on the first crack section	103
2.8.A.	Spring support stiffness input for <i>Well tamped sides</i>	104
2.8.B.	Principal stress distribution in x-direction and crack pattern	105
2.8.C.	Load-deflection at first crack point	105
2.8.D.	Vertical deflection along the sleeper length at different load stage	106
2.8.E.	Principal stress in x-direction on the first crack section	106
2.9.A.	Spring support stiffness input for <i>Stabilized rail seat and sides</i>	107
2.9.B.	Principal stress distribution in x-direction and crack pattern	108
2.9.C.	Load-deflection at first crack point	108
2.9.D.	Vertical deflection along the sleeper length at different load stage	109
2.9.E.	Principal stress in x-direction on the first crack section	109
2.10.A.	Spring support stiffness input for <i>Uniform pressure</i>	110
2.10.B.	Principal stress distribution in x-direction and crack pattern	111
2.10.C.	Load-deflection at first crack point	111
2.10.D.	Vertical deflection along the sleeper length at different load stage	112
2.10.E.	Principal stress in x-direction on the first crack section	112
3.A.	Relevant information from KTMB's Double Track Specification	113
3.B.	Dynamic Wheel Load	113
3.C.	Rail seat load	114
3.D.	Results from Testing of Prestressed Concrete Sleeper (DNV,2002)	115

CHAPTER 1

INTRODUCTION

1.1. MODERNIZATION OF THE BALLASTED RAILWAY TRACK NETWORK IN MALAYSIA

The Government of Malaysia through Keretapi Tanah Melayu Berhad (KTMB) is embarking on an exciting challenge in modernizing its ballasted railway track through the implementation of double tracking and electrification of its railway system on the west coast of the peninsular.

This includes the already completed Rawang-Ipoh Project, the ongoing Ipoh-Padang Besar Project and the Seremban-Gemas Project as well as the upcoming Gemas-Johor Bahru Project. Total project cost of the modernization of this ballasted railway track is approximately RM 30 billion.

The modernized ballasted track is designed to replace the colonial track of 90 km/h top speed with the 140 km/h maximum operational speed which could go up to its limit of 160 km/h on certain stretches. This will directly reduce the transit time for both passengers and goods traffic which in return will stimulate developments and economic growth along its corridor.

Once the network between Johor Bahru and Padang Besar is completed, it will further spur and enhance the growth of international container traffic through train services between the ports of Malaysia. It will definitely pave the way for the success of the Indonesia-Singapore-Malaysia-Thailand Growth Region.

1.2. FUNCTIONS OF TRACK COMPONENTS AND THE LOAD PATH

The design of a railway system is typically divided into two main components namely the design of trains or rollingstock and the design of the supporting structure (Remennikov, Kaewunruen, 2008). It is expected that the track structures will guide and facilitate the safe, economic and smooth passages of any passenger and freight trains.

By considering the static and dynamic loads acting on the track structure, railway track structures is primarily analysed and designed to avoid excessive loading which may induce damage to the track substructure and superstructure. This include track components such as rails, rail pads, mechanical fasteners and concrete sleepers (superstructure) as well as geotechnical systems such as ballast, sub-ballast and subgrade or formation (substructure). Fig. 1.1 shows the cross sectional layout of a typical ballasted track (Selig & Waters, 1994).

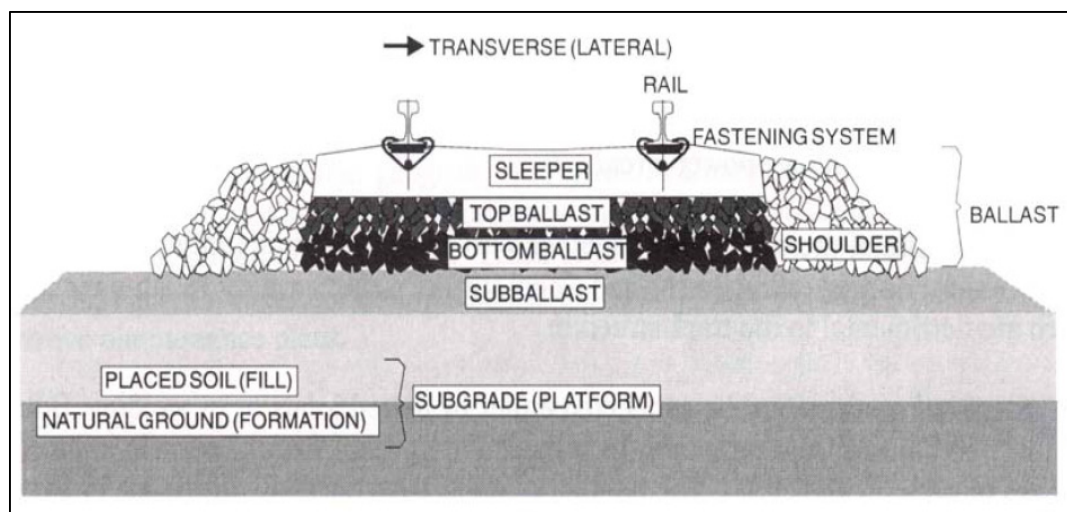


Figure 1.1: Cross sectional layout of a typical ballasted track (Selig & Waters, 1994)

As a longitudinal steel members positioned on the equally spaced sleepers, rails are the critical component in guiding the rolling stocks. Its main function is to accommodate and transfer the loads from the rolling stock to the supporting sleeper. With adequate strength and stiffness in the rails, a steady shape and smooth track is maintained and various forces exerted by travelling rolling stocks are resisted. In modern electrified track, rails had additional function of serving as an electrical conductor for railway signaling system.

Both mechanical fasteners and rail pads are the primary components of the fastening systems. Apart from keeping the rails in position on the sleepers, the mechanical fasteners withstand the three dimensional forces of vertical, lateral and longitudinal as well as the overturning movements of the track. Mechanical fastener also transfer forces caused by wheels, thermal change and natural hazard from rails to the adjacent set of sleepers.

As the other primary components of the fastening systems, rail pads which are placed on the rail seat are essential in filtering and transferring the dynamic forces from the rails and mechanical fastener to the sleepers. The dynamic force is predominantly from the travelling rolling stocks and the high damping coefficient of the rail pads considerably reduces the excessive high-frequency force components to the sleepers. The resiliency provided by the rail pads to rail-sleeper interaction has resulted in the alleviation of rail seat cracking and contact attrition.

Sleepers are part of the track component that rest transversely on the ballast with respect to the longitudinal rail direction. It was first made using timber before evolving to steel, reinforced concrete and to the most common type seen today, prestressed concrete. This evolution is closely related to improve durability and longer service life span. In terms of its functionality, sleepers are critical in (i) providing support and restraint to the rail in vertical, longitudinal and lateral direction, (ii) transferring load from the rail foot to the underlying ballast bed, and (iii) retaining proper gauge and inclination of the rail by keeping anchorage for the rail fastening system.

Underneath the sleepers in providing tensionless elastic support is ballast, a free-draining coarse aggregate layer typically composed of crushed stones, gravel, and crushed gravel. Depending on the local availability, basalt and granite are usually the selected material for ballast due to its strength characteristic for load transfer. In between the ballast and the underlying subgrade is sub-ballast, commonly composed of broadly graded slag, broadly sand-gravel or crushed aggregate. The last support to sustain and distribute the resultant downward dynamic loading along its infinite depth is subgrade or also known as formation. Subgrade includes existing soil and rock as well as other structures such as pile embankment and the recent high performance materials of geotextiles and

geofabrics. To prolong track serviceability, the infinite depth of subgrade must have adequate bearing capacity, provide good drainage and yield tolerable smooth settlement.

1.3. PROBLEM STATEMENT

As reviewed by Doyle (1980), one of the main functions of prestressed concrete sleepers is to transfer the vertical loads to the ballast and formation. This vertical loads subject the sleeper to bending moment which is dependent on the pressure distribution exerted by the ballast underneath the sleeper.

In practice, a uniform pressure distribution is assumed in design to calculate the static load capacity of the sleeper in withstanding the bending stresses. This also lead to a four point bending moment test at the rail seat in the laboratory (AS 1085.14-2003) based on the assumption that the sleepers would behave similar to those of the in-situ ones. (Remennikov, Murray, Kaewunruen, 2008)

However, this assumption is not completely true as the bearing pressure distribution on the sleeper-ballast interaction is mainly depending on the degree of voids in the ballast underneath the sleeper. The major influence factors in determining the degree of voids are the traffic loading and train speed. Both factors are time dependent as cumulative effect of the traffic loading at various speeds will gradually change the structure of the ballast and the subgrade. A remarkable effort by Talbot (1913-1940), other researchers and standards have postulated a set of hypothetical bearing pressure distribution on the sleeper-ballast interaction and their corresponding bending moment diagrams.

Therefore, quantifying the rail seat load and the bearing pressure distribution is the most critical steps in designing the sleeper to withstand vertical loading. Numerical analysis using a commercial finite element package, LUSAS, was carried out to check on the assumption made on the laboratory test as well as to check whether the assumption of uniform pressure will provide an overestimate of

the sleeper's static load capacity in relative to other hypothetical bearing pressure distribution.

The preliminary applied rail seat load in the design and numerical analysis will be based on 20 tonne axle load which is the maximum imposed load as regulated by the Malaysian Railway Authority although it is acknowledged excessive wheel load over 400 kN due to wheel or rail abnormalities may occur once or twice in the sleeper's design life span of 50-100 years (Kaewunruen, Remennikov, 2009). This is considered a rare event and it is not economic to design sleeper for such a high static load capacity.

Subsequently, the rail seat load will be increased if the bending stress limit is not exceeded. If the bending stress is exceeded prior to rail seat load based on 20 tonne axle load, a lower load will be applied to predict what load the sleepers will fail under flexure.

1.4 . OBJECTIVES OF THE STUDY

The objective of this study are :

- a) To develop two-dimensional model of prestressed concrete sleepers using finite element analysis modelling;
- b) To compare the finite element analysis model with the load-deflection response of the centre negative moment experimental test as previously conducted by Kaewunruen and Remennikov (2006a);
- c) To verify if the assumed uniform bearing pressure distribution on the sleeper-ballast interaction is not underestimating the design if other hypothetical bearing pressure distribution pattern occurs;
- d) To predict the maximum vertical static loading capacity at crack initiation stage and ultimate state on various hypothetical bearing pressure distribution patterns.

1.5. SCOPES OF THE STUDY

The scope of this study are :

- a) To review the analysis and design of monoblock prestressed concrete sleepers by referring to Section 4 of AS 1085.14-2003 as practiced by the track designer of KTM Double Track Projects;
- b) To perform numerical analysis using finite element software, LUSAS, with various hypothetical bearing pressure distribution on the sleeper-ballast interaction as the controlled variable.
- c) To apply specification of sleeper dimension, rail seat loading, material properties and other technical parameters based on the centre negative bending moment test carried out by Kaewunruen and Remennikov (2006a). The ballast stiffness will be based on technical specification used in KTM Double Track Project.
- d) To only consider quasi-static wheel loads in the full scale experiments and numerical analysis, impact loads are omitted.
- e) To only consider independent, closely spaced, discrete and linearly elastic springs for the beams on elastic foundation. Continuum approach is omitted as effects on local pressure distribution are assumed negligible in the transverse direction of the track.